CrossMark

ORIGINAL RESEARCH PAPER

Optimal design of isolation devices for mid-rise steel moment frames using performance based methodology

Jian Zhang[1] · **Zhan Shu**[2]

Abstract This paper develops and applies the performance-based analysis and design methodology to assess the seismic vulnerability of mid-rise steel moment frame structures and to optimally design the isolation devices to reduce the direct losses due to earthquake damages. An isolated steel moment frame, originally tested in the 2011 E-Defense blind prediction contest, is selected and modeled in detail. The numerical model and the predicted seismic responses of the structure are validated against the full-scale shaking table test results. Subsequently, the fragility functions are derived for the structure when subject to near-fault ground motions exhibiting distinctive acceleration or velocity pulses and far-field motions with less impulsive characteristics. To quantify the system level damage states of the building, the concept of total loss ratio (*TLR*) is applied as the performance index to account for the direct loss due to structural, non-structural and isolation components in relation to the total repair cost of the original structure. The *TLR* considers the failure probability (as defined by fragility functions), the damage percentage and related cost for each damage state. Finally, among various isolation designs, the optimal configuration is derived for cases with the minimum *TLR*. It is shown that the optimal design can reduce the *TLR* up to 90% of that of the un-isolated structure and it also outperforms the adopted design in the test program. The study demonstrates a systematic way of achieving the optimal isolation design with considerations of uncertainties in earthquake inputs and the combined structural and non-structural damages.

Keywords Steel moment frame · Performance based design · Base isolation · Optimal design · Total loss ratio · Fragility functions

✉ Zhan Shu
shuzhan@tongji.edu.cn

Jian Zhang
zhangj@ucla.edu

1 Department of Civil and Environmental Engineering, University of California, Los Angeles, CA 90095, USA

2 Department of Structural Engineering, Tongji University, Shanghai 200092, China

⚫ Springer

1 Introduction

Seismic protective devices in the form of passive or semi-active can be used to mitigate the direct and indirect seismic losses to buildings (Lafontaine et al. 2009; Lee et al. 2006). Among which the base isolation system has been proved as an effective passive system to dissipate and deflect earthquake input energy through lengthening the fundamental structural period to avoid the dominant frequency of ground motions (Kelly 1986; Skinner et al. 1993). For the steel moment frames (SMF), the base-isolation technique becomes more favorable as it provides sufficient structural damping, which is not usually provided by the superstructure itself. To design an isolation system, although the current building design codes (e.g. ASCE 7-10 2010) provide descriptive methods, they cannot incorporate uncertainties inherent with ground motion characteristics, building modeling parameters (e.g. material properties, member stiffness and strength), capacity estimations, and variations in geometric irregularities of buildings, etc. More importantly, the isolation design cannot be directly related to the expected performance of buildings.

To further define and quantify the structural performance, the performance-based design and analysis methods emerged. The concept was formally established in SEAOC Vision 2000 document (1995) and further developed in several design documents (e.g. ATC-40 1996; FEMA 273 1997a; FEMA 274 1997b; ATC-58 2012, etc.). The methodology intends to logically quantify the seismic hazards and link predictable/measurable performance requirements to design decisions based on damage levels. The outcome of the methodology is often the estimated frequency (in probability sense) with which a particular performance metric will exceed various levels for a given design at a specific location. For the SMFs, nonlinear drift estimations that are often used to define the performance levels were provided (Sabelli et al. 2003). In addition, Haselton et al. (2007) produced an analysis and design methodology for a benchmark moment frame building to address its seismic performances in terms of damage-repair cost, loss-of-use duration, as well as operability, life-safety, and collapse potential.

Such performance based earthquake engineering (PBEE) framework is particularly useful in the case of base isolation design when the device parameters can be directly related to a probabilistic performance index, which facilitates the comparison of different isolation designs. For example, Sayani and Ryan (2009) developed a response index to compare the relative performance of many systems and to predict the best system to achieve a given performance objective for both base-isolated and fixed-base buildings. Zhang and Huo (2009) developed a performance index considering both column and isolator damage for isolated highway bridges. Recently, researchers presented the total seismic loss as an intuitive performance index by providing the expected losses to stakeholders (Aslani and Miranda 2005; Dhakal and Mander 2006; Solberg et al. 2008; Bai et al. 2009; Graf and Lee 2009; Shu et al. 2017). To estimate the loss to a specific building, the damage is usually categorized into different components such as structural and non-structural damage. Damage to each of these components is evaluated in terms of percentage of the replacement cost of the component. Most current loss approaches use probabilistic integrated methodologies such as fragility curves to estimate the losses due to structural and non-structural damage (i.e. combines fragility curves with loss functions). However, not many existing studies have applied the PBEE framework for the structural design considering the total loss.

This paper adopts the performance-based methodology to evaluate the effectiveness and optimum design parameters of isolation devices for a SMF such that the overall damaging potential of seismically isolated building system is minimized. The concept of total loss

ratio (*TLR*) is implemented to account for the direct loss due to both structural and non-structural damage in relation to the total repair cost of the original structure. By relating fragility functions at different damage states to the total loss ratio, isolation devices with various mechanical properties can be evaluated under this probabilistic framework to derive the optimal design based on the minimum damage probability in terms of the *TLR*. Following a brief introduction of PBEE framework to derive fragility functions of defined damage states, the paper presents the loss model based on the *TLR*. This is then applied to a five-story steel moment resisting frame building to derive its fragility curves for both un-isolated and isolated cases. The numerical model for the building was developed and calibrated with the shake table test data. Subsequently, a detailed parametric study of various isolation parameters is conducted and the *TLR* is obtained to serve as the criteria for evaluating the merit of each design. Finally, the optimal design range for isolation devices is determined.

2 The fragility function methodology and the loss assessment

The performance based approach involves four stages: hazard analysis, structural analysis, damage analysis, and loss analysis (Porter 2003). In the hazard analysis, one evaluates the seismic hazard ($\lambda[IM]$), which describes the annual frequency with which seismic excitation is estimated to exceed various levels. Seismic excitation is parameterized by an intensity measure (*IM*) such as spectral acceleration at fundamental period of structure ($Sa(T_1)$), peak ground acceleration (PGA), peak ground velocity (PGV), and magnitude (Zhang and Huo 2009; Mackie and Stojadinović 2007). In the structural analysis, one creates a structural model to estimate the uncertain structural responses, measured in terms of a vector of engineering demand parameters (*EDP*), conditioned on seismic excitations (i.e. $p[EDP|IM]$). *EDP* is then the input to a set of fragility functions that model the probability of various levels of physical damage (expressed by damage measures, or *DM*), conditioned on structural responses (i.e. $p[DM|EDP]$). Physical damage is described at a detailed level, defined relative to particular repair efforts required to restore the component to its undamaged state. The last stage in the analysis is the probabilistic estimation of performance (parameterized by various decision variables, *DV*), conditioned on the damages (i.e. $p[DV|DM]$). *DV*s measure the seismic performance of the building in terms of greatest interest to facility owners, whether in dollars, deaths, downtime, or other metrics. The loss models for repair cost are often based upon well-established principles of construction cost estimation.

2.1 Selected ground motion ensembles

A sufficient number of earthquake records need to be selected for the fragility analyses to obtain conceptually and statistically better building response predictions. Researchers in the past may either artificially generate ground motions or collect them from historical events that represent typical and severe earthquake events (Ryan and Chopra 2004). In this study, three ensembles were collected with a total of one-hundred motions that represent pulse-type (near-fault) motions and non-pulse-like (far-field) motions. The first two ensembles are the acceleration and velocity pulse motions identified by Tang and Zhang (2011), representing ground shakings relatively closer to fault rupture during some larger earthquakes. The third ensemble collects another 50 far-field earthquake records

representing non-pulse-like ground motions. The three ground motion ensembles represent events with various probability of occurrence at different locations and occurring on firm soil conditions.

As the ground motions are characterized by the user-defined *IM*s, the choice of *IM* plays a crucial role in both running the fragility analysis and interpreting simulation results. With the suggestion by Mackie and Stojadinović (2005), in a logarithmic reference frame, the linear consistency of the results from probabilistic analysis can be an indicator of the applicability of the *IM*, which is used to interpret the results. Based on this criterion, the PGA and PGV are good choices of *IM* for relating to the *EDP* measures. This study chooses PGA as the ground motion *IM* based on their efficiency, practicality, sufficiency and hazard computability compared with other *IM*s (Padgett et al. 2008). In addition, $Sa(T_1)$ is not used in this study as the fundamental period of the isolated structure is changing, which is determined by the effective period of the isolation system.

Figure 1a, b shows the averaged acceleration spectra with 5% damping for pulse-type (red dash-dotted lines), far-field (blue dotted lines) and all 100 motions (black solid line) at the fault normal (left) and fault parallel (right) directions, respectively. Since the PGA is selected as the *IM*, its distribution among all 100 motions is shown Fig. 1c. The averaged PGAs are 0.480, 0.571 and 0.147 g for acceleration pulse-type, velocity pulse-type and far-field motions, respectively. In addition, the averaged PGA for all the motions is 0.336 g. The ground motions are carefully selected to represent the second level—severe level
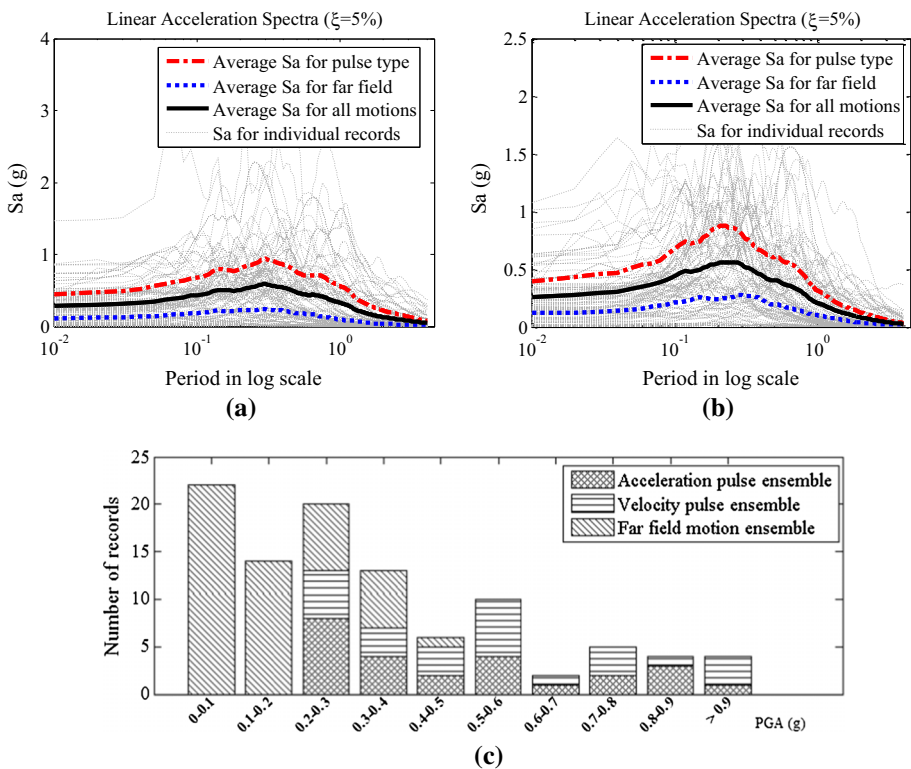

Fig. 1 Information of selected ground motion ensembles and the spectra: **a** acceleration spectra along FN direction, **b** acceleration spectra along FP direction, **c** PGA distribution

ground motion in Japan. The selection is based on the target spectrum. Correspondingly, the PGAs of the selected motions are within the neighborhood generally considered for the severe level. With the selected motions, no scaling is needed for the fragility analyses, which is introduced in detail in the subsequent section.

2.2 The fragility function methodology

The fragility function methodology serves as the foundation of the proposed loss estimation model in this paper. Typically, a fragility curve defines the conditional probability of attaining or exceeding a (or several) specified damage state(s) (*DS*) for a given set of ground motion intensity measures. The fragility curves are commonly generated by the incremental dynamic analysis (IDA) or the probabilistic seismic demand analysis (PSDA) (Zhang and Huo 2009). This paper adopts the PSDA method, where cloud approach (i.e. using un-scaled earthquake ground motions) is used for nonlinear time history analysis and the regression analysis is applied to obtain the mean and standard deviation for each limit state (*LS*) by assuming the logarithmic correlation between the median *EDP* and an appropriately selected *IM*:

$$EDP = a(IM)^b \tag{1}$$

where the parameters *a* and *b* are regression coefficients obtained from the response data of nonlinear time history analyses. For the PSDA analyses, the aforementioned ground motions ensembles are used without scaling. Besides, the structural modeling details are provided in the subsequent sections. By taking the logarithmic of above equation, one arrives at:

$$\ln(EDP) = \ln a + b \ln(IM) \tag{2}$$

The provided equation is a linear regressed equation between ln(*EDP*) and ln(*IM*) based on the calculated response distribution. The regression analyses aims at the smallest standard deviation $\sigma_{EDP|IM}$, which could be estimated as:

$$\sigma_{EDP|IM} = \sqrt{\frac{\sum_{i=1}^{n} \left[\ln(EDP_i) - (\ln a + b \ln(IM_i)) \right]^2}{n-2}} \tag{3}$$

where *n* is the total number of *EDP* responses (here is also the number of earthquake records) and *i* is the index of each individual record from 1 to *n*. Subsequently, a capacity model uses the *EDP*s or functions of *EDP*s to derive the damage index (*DI*) that can be compared with the *LS*s correspondent to various dictated *DS*s. For simplicity, the *DI* for each structural component (SC) is chosen the same as the *EDP* in this study. By further assuming a lognormal distribution of *EDP* at a given *IM*, the fragility functions (i.e. the conditional probability of reaching a certain damage state for a given *IM*) can be written as:

$$p[DI \geq LS|IM] = 1 - \Phi \left(\frac{\ln(LS) - \ln(aIM^b)}{\sigma_{EDP|IM}} \right) \tag{4}$$

where $\sigma_{EDP|IM}$ is the standard deviation of the logarithmic distribution computed from Eq. (3) and $\Phi(\bullet)$ is the standard normal distribution function. Alternatively, the fragility function can be deployed as:

$$p[DI \geq LS|IM] = 1 - \int_0^{LS} \frac{1}{\sqrt{2\pi}\sigma_{EDP|IM}} e^{\frac{[\ln(EDP)-\ln(aIM^b)]^2}{2(\sigma_{EDP|IM})^2}} d(\ln(EDP)) \qquad (5)$$

With the provided linear regression analyses in the logarithmic space, and the computed standard deviations, the fragility functions could be easily generated as it follows the standard cumulative normal distribution.

2.3 Damage index and damage states for isolated steel moment frame

The capacity models, which are described in terms of a *DI* as a function of *EDP*s, are commonly used to measure the damages states. For general building inventory, FEMA (2003) presented the *HAZUS-MH MR4 Technical Manual*, which provides typical *DS* definitions and the performances for various design codes were evaluated. The HAZUS manual defines four different earthquake damage levels, namely the slight, moderate, extensive and complete damages. In addition, buildings are categorized to high-, moderate-, and low-code seismic design standards, or not seismically designed (i.e. the pre-code buildings).

For building structures, both structural and non-structural components (NSC) can be vulnerable to earthquake damages. The NSC damage (i.e. building contents) often represents the majority portion of the total repair cost after earthquake (Yun et al. 2002). The SCs include load resisting members of superstructure (e.g. beams and columns). Their damage levels correlate well with curvature or displacement/inter-story drift etc. (Williams et al. 1997; Fajfar and Gašperšic 1996). In addition, the plastic displacement and the ductility demand are shown to be reliable indicators of severe damage to structural members (Kircher 2003). In addition, since the non-structural damages can be triggered by the response intensities lower than those required to produce structural damages, they are necessary to be included in the overall loss assessment of buildings. The NSCs could be categorized to the drift sensitive NSCs and the acceleration sensitive NSCs. According to *HAZUS-MH MR4 Technical Manual*, most of the NSCs are sensitive to the floor accelerations. Consequently, the inter-story drift is selected as the damage index for structural damage while the maximum top floor acceleration is selected to quantify the non-structural damages. To consider the drift sensitive NSCs such as the partition walls, the veneer and finishes, and the penthouses potentially available for the SMFs, the study slightly increases the cost of the SCs provided in the subsequent sections.

It is noted that base isolation can reduce the floor accelerations hence can minimize the nonstructural damages (Lafontaine et al. 2009). Meanwhile, the isolation devices of isolated buildings can also experience large horizontal drifts, leading to the damages of the isolation devices and their neighboring structural members (Hall et al. 1995). Existing studies usually relate the damages of the bearings with their shear strain, displacement or drift (Zhang and Huo 2009). In this study, the bearing shear strain is selected to quantify the damages to the isolation system. Therefore, three *EDP*s, namely the peak inter-story drifts, the maximum floor accelerations, and the bearing shear strains, are selected to evaluate the performance of isolated buildings. Finally, to keep the study simple, collateral damages and the interconnected damages are not considered in this study.

A mid-rise steel moment frame is selected subsequently as an example to implement the proposed PBEE framework. According to the FEMA definition (2003), the sample structure is categorized into S1 M category and the four *DS*s for S1 M type buildings are given in the document. The slight damage is defined when minor deformations in connections or

hairline cracks in welds occur. The moderate damage state is the observation of some yielded steel members exhibiting observable permanent rotations at connections; few welded connections may exhibit major cracks through welds or few bolted connections may exhibit broken bolts or enlarged bolt holes. The extensive damage, arrives when most steel members have exceeded their yield capacity, flanges buckle and connections fail. The final state of complete damage happens when significant portion of the structural elements have exceeded their ultimate capacities or some critical structural elements or connections have failed resulting in dangerous permanent lateral displacement, partial collapse or collapse of the building. Table 1 summarizes the inter-story drift performance level of a mid-rise SMF at threshold of damage states while Table 2 summarizes the absolute floor acceleration used in subsequent sections at threshold of damage states for NSCs.

As the sample structure belongs to the moderate code seismic design level, Table 3 lists the four *DS*s and their corresponding damage indexes (i.e. the limit *EDP*s) for the subsequent analyses. Specifically, as the bearing damages have not been defined by FEMA, their shear strain damage states used in this study are referred from the study by Zhang and Huo (2009). The damage states are defined such that they are generally suitable for most of the isolation systems. For the triple pendulum bearings, for example, in the work by Fenz and Constantinou (2008), for a 50-mm height isolator according to the design, the second stiffening effect become fairly large at 140 mm. The isolator could not afford much more displacement after this amount due to a locked situation incurring damage to the isolator itself. This displacement corresponds to an equivalent "shear strain" between 250 and 300%, which is around the neighborhood of the 250% (defined as the complete damage state). Therefore, assuming the damage state 100, 150, 200, 250% for the slight, moderate, extensive, and complete damage is a fair statement, which quantitatively defines the performance of isolation at the system level for the generalized isolation systems.

2.4 The loss assessment

After obtaining the damage indexes for individual components, the component damage states can be determined. However, a comprehensive *DS* incorporating the component level damages is needed to derive the system level fragility. Previous studies suggest that system fragility can be derived based on the functionality or repair cost after earthquakes (Mackie and Stojadinović 2005) or be generated as a union of the component level fragility using a joint probabilistic seismic demand model (Nielson and DesRoches 2007). In this study, a probabilistic loss model is inherited from FEMA documentations to quantify the system level damage state (FEMA 2003). It directly relates earthquake hazard to building responses and subsequently to total losses in the form of the repair cost ratio. This loss

Table 1 Inter-story drift ratios for structural damage states (FEMA 2003)

	Slight	Moderate	Extensive	Complete
High-code seismic design level	0.0040	0.0080	0.0200	0.5333
Moderate-code seismic design level	0.0040	0.0069	0.0157	0.0400
Low-code seismic design level	0.0040	0.0064	0.0135	0.0333
Pre-code seismic design level	0.0032	0.0051	0.0108	0.0267

Table 2 Floor acceleration for non-structural damage states (unit: g) (FEMA 2003)

	Slight	Moderate	Extensive	Complete
High-code seismic design level	0.30	0.60	1.20	2.40
Moderate-code seismic design level	0.25	0.50	1.00	2.00
Low-code seismic design level	0.20	0.40	0.80	1.60
Pre-code seismic design level	0.20	0.40	0.80	1.60

Table 3 The damage states and the damage indexes for sample steel moment frame

Description		Percentage damage	Accel. (non-str.) (g)	Disp. (str.) (%)	Bearing shear strain (iso.) (%)
1	Slight	2	0.25	0.40	100
2	Moderate	10	0.50	0.69	150
3	Extensive	50	1.0	1.57	200
4	Complete	100	2.0	4.00	250

estimation framework is also closely tied with the component fragility functions and is compatible with the overall PBEE framework presented above.

The total loss ratio (*TLR*) is the cost of earthquake repairs as a percentage of the replacement value of the original building cost. It has been proved to be a useful performance index to civil structures (Shu et al. 2017). For a base-isolated structure, the *TLR* is defined by Eq. (6):

$$TLR = \frac{c_{st} \sum_{i=1}^{4} P_{(i)}^{st} r_{(i)}^{st} + c_{ns} \sum_{i=1}^{4} P_{(i)}^{ns} r_{(i)}^{ns} + c_{iso} \sum_{i=1}^{4} P_{(i)}^{iso} r_{(i)}^{iso}}{c_{st} + c_{ns} + c_{iso}} \tag{6}$$

where $i = 1$–4 stands for the four damage states. $r_{(i)}^{st}$, $r_{(i)}^{ns}$, and $r_{(i)}^{iso}$ are the percentage damaged for each of the damage state for SCs, NSCs, and isolation system with detailed values presented in Table 3. The c_{st}, c_{ns} and c_{iso} stands for the original cost for the three components. Notice that c_{st} shall also include the cost of the drift sensitive NSCs, if there is any. Besides, $P_{(i)}^{st}$, $P_{(i)}^{ns}$, $P_{(i)}^{iso}$ are the probabilities that are bounded by the four fragility curves within each fragility curves of these three components. In addition to the damage indexes for structural, non-structural and isolation devices, Table 3 also lists the damage percentage corresponding to four damage states as part of the loss model. The damage percent increases as the damage states progress. In addition, this loss model has been roughly calibrated and validated with building design documents (e.g. ATC-40 1996) and cost data collected from the construction practice (Plotner et al. 2016).

To simplify the calculation, one could assume that SC has a value of *A*, and the other two categories cost *αA* and *βA*, respectively. The total replacement cost of the isolated building is therefore the sum of cost for each component [i.e. $(1 + \alpha + \beta)A$]. Notice that a demolition cost should also be added to the total cost. The coefficients *α* and *β*, are obtained based on previous observations and value estimations of total NSCs and isolation system. The value of *α* varies with different types of building according to their functions and placement of acceleration sensitive components. For this study, *α* values of 0, 50 and

100% are chosen and studied to account for different situations that might happen in the SMF. β is set to 8% in this study as the total cost for base isolation devices, which is usually within 10% of the structural cost (i.e. the upper bound of β). Equation (6) can be rewritten as:

$$TLR = \frac{\sum_{i=1}^{4} P_{(i)}^{st} r_{(i)}^{st} + \alpha \sum_{i=1}^{4} P_{(i)}^{ns} r_{(i)}^{ns} + \beta \sum_{i=1}^{4} P_{(i)}^{iso} r_{(i)}^{iso}}{1 + \alpha + \beta} \qquad (7)$$

Following the introduced PBEE procedure, fragility curves can be derived for each component based on three *EDP*s (i.e. the maximum inter-story drift for structural damage, the absolute maximum top floor acceleration for non-structural damage, and the shear strain for isolation devices). As schematically sketched in Fig. 2, each component is bounded by four fragility curves. Since the repair cost of the higher damage states have already included the repair cost of the lower damage states, the probabilities of each damage state in Eqs. (6) and (7) are computed as the difference between the conditional probabilities of the bounding fragility curves. For each of the three components (e.g. SCs), probability values ($P_{(1)}$, $P_{(2)}$, $P_{(3)}$, and $P_{(4)}$) that correspond to each performance level can be obtained for a given *IM* from the fragility curves and they satisfy $0 \leq \sum_{i=1}^{4} P_{(i)} \leq 1$. The following case study demonstrates the entire process of calculation *TLR* based on the fragility curves for each component.

3 The isolated steel moment frame: case study

In order to demonstrate the developed methodology, an experimentally tested fixed-base steel building and its retrofitted counterpart using base isolation are selected. The shake table tests were conducted on the largest earthquake simulator at E-Defense in Japan (Ji et al. 2013; Yu et al. 2010, 2013). The structure was also the subject of the Blind Prediction Contest (2011). Consecutive numerical studies have also been done based on the tested data to explore the structural seismic responses as well as the effectiveness of the passive

Fig. 2 Illustration of bounded probability in percentage for each state
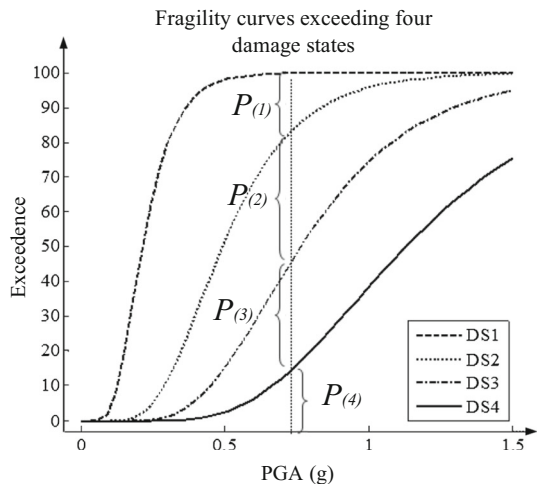
control devices (Yu et al. 2010; Dao and Ryan 2014). In this section, numerical models are developed and the fragility curves are derived for the fixed-base and isolated steel building.

3.1 Structure information

The layout of the 5-story steel building structure could be found in the Blind Prediction Contest (2011). Shown in Fig. 3, it consists of a two bay by two bay plane with 7000- and 5000-mm span in X direction and two 5000-mm spans along the Y direction. This study assumes "Y direction" (in Fig. 3) as the weaker yet major direction, and "X direction" as the stiffer yet secondary direction. Figure 3a shows the elevation view of the frame with a 3850-mm tall first story and four 3000-mm tall stories above. Figure 3b shows the plan view also in the unit of mm. The structural elements are designed to withstand potential strong ground motions in Japan. Further information of the building could be obtained from the work from Tokyo Institution of Technology (Kasai et al. 2011). The numerical model for the building follows a bilinear hysteretic behavior, which is characterized with elastic stiffness K_{1_B}, post-yielding stiffness K_{2_B} and characteristic strength Q_{d_B}. The static pushover analysis (Fig. 3c) reveals that the bilinear parameters along the major direction of the designed building are $K_{1\_B} = 25$ MN/m, $K_{2\_B} = 1750$ kN/m, and $Q_{d\_B} = 4194$ kN, where "B" stands for the building in the subscript. The story weights are 842, 841, 822, 816, 798, and 1153 kN from the ground level to the roof level respectively which adds up to 5309 kN above the isolation system. The first modal period T_1 is 0.65 s. In addition, assuming all diaphragms are rigid, the first seven natural frequencies of the building are 1.52, 1.58, 1.87, 4.81, 4.98, 5.87, and 9.35 Hz respectively. The torsional mode for the story diaphragms is the sixth mode, which is considered insignificant for this structure.

The tested base-isolated structure is seated on nine friction pendulum bearings. The bearings are triple pendulum isolators with two inner sliding surfaces and two outer sliding surfaces with their sectional geometry and elevation view demonstrated in Fig. 4a (provided with permission from the related authority). All of the bearings have been lab tested and the test result for one of the bearings is shown in Fig. 4b (provided with permission from the related authority) where a bilinear behavior generally captures the force–displacement relationship within the tested displacement range. Based on this information, the originally designed isolators can be assumed to have bilinear responses and their pre-yield and post-yield stiffnesses are $K_{1\_I} = 35$ MN/m, $K_{2\_I} = 760$ kN/m, and $Q_{d\_I} = 386$ kN, where "I" stands for the isolation system in the subscript. The strength in terms of building
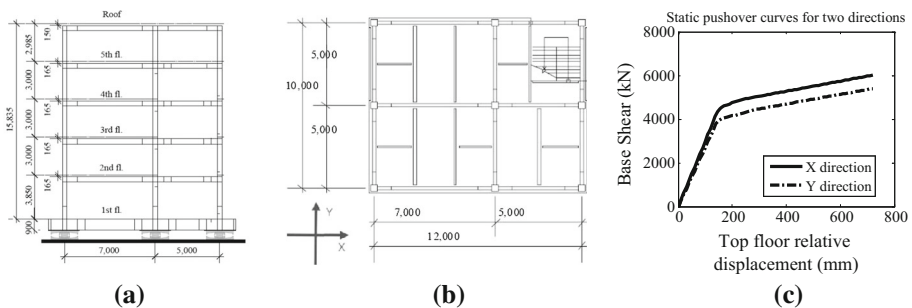

Fig. 3 Structural information of full-scale 5-story steel MF building: **a** elevation view of the tested steel structure, **b** plan view of the tested steel structure, **c** two directional pushover curves
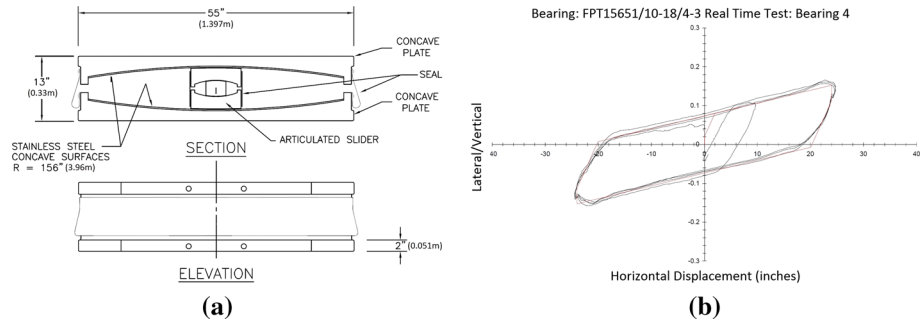
Fig. 4 Triple pendulum isolation system and their tested behavior: **a** section and elevation of a tested TFP bearing, **b** tested result of TFP bearing and its equivalent bilinear behavior

weight is 7.27%. The stiffness ratio between the pre-yielding stiffness K_{1_I} and post-yielding stiffness K_{2_I} is measured by a parameter $N = K_{1\_I}/K_{2\_I}$. For the model representing the tested pendulum isolator design, the stiffness ratio N is about 46. The effective isolation period of the structure is around 2.19 s when the isolators experience 100% shear strain. Besides, the effective isolation period at 200% shear strain is 2.87 s (considering the hardening effect) and 3.10 s (ignoring the hardening effect). In addition, the inelastic features of the isolation system compared with that of the superstructure corresponds to $Q_{d\_I}/Q_{d\_B} = 9.2\%$ and $K_{1\_I}/K_{1\_B} = 1.4$ approximately.

Moreover, not provided in the figure, the hardening behavior could be expected at a larger strain level for the triple pendulum bearings, stiffening the isolated layer of the building (Fenz and Constantinou 2008). Makris and Vassiliou (2011) discovered similar responses between the friction bearing with two sliding surfaces and a bilinear behavior with the initial stiffness and post-yielding stiffness matching the 1st and 3rd segmental stiffness of the triple pendulum isolators. Consequently, parallel to the bilinear behavior, a nonlinear elastic hardening behavior was added in the numerical simulation after 150% isolator shear strain while modeling the triple pendulum isolators. The hardening element makes the triple pendulum isolators very stiff at nearly 250% shear strain representing a locked condition.

Although the designed and tested isolators for the building are triple pendulum bearings, other types of isolators can also be used for base isolation design. In current practice, three types of isolators are commonly used: elastomeric bearings (ERB) (Kumar et al. 2014), lead-rubber bearings (LRB) (Kalpakidis et al. 2010), and friction pendulum systems (FPS) (Kelly 1986). In addition, new types of isolation systems have been invented and tested over the decades such as the fiber-reinforced elastomeric isolators (Moon et al. 2002). Nonetheless, the generalized hysteretic behavior of isolation system is close to bilinear (Naeim and Kelly 1999). Therefore, to represent the hysteresis behavior of isolation system in a broader sense, the bilinear behavior is assumed for the generalized isolation systems. Features for special isolators such as the hardening effect of the triple pendulum isolators are consequently not considered in the subsequent system level study. Table 4 summarizes the parameters and formulas for bilinear modeling of these three isolation devices. In the subsequent parametric study, various isolation devices with different K_1, K_2 and Q_d have been selected to determine the optimal design of the isolation system.

Table 4 Formulas of bilinear modeling for the typical isolation devices (Zhang and Huo 2009)

	Elastic stiffness, K_1	Characteristic strength, Q	Post-yielding stiffness, K_2
ERB	$K_1 = NK_2$ ($N = 5$–15)	From hysteresis loop	$K_2 = GA/\sum t_r$
LRB	$K_1 = NK_2$ ($N = 15$–30)	$Fy = f_y A_{Lead}$	$K_2 = (1.15$–$1.20)GA/\sum t_r$
FPS	$K_1 = NK_2$ ($N = 50$–100)	$Q = \mu W$	$K_2 = W/R$

3.2 Modeling of the isolators

In additional to the rate independent bilinear behavior, Casciati (1989) considered the Bouc–Wen model (Bouc 1971; Wen 1975, 1976) as a smoothed form of the bilinear model and generalized it to the bi-directional case. The Bouc–Wen model was proved an accurate model for the steel elements and the isolation system. This paper implements the bi-directional coupled bilinear and Bouc–Wen model into the software platform OpenSees (2017). The implementation of the bi-directional Bouc–Wen model was documented by Makris and Zhang (2002) in detail. According to this model, restoring force $\mathbf{P} = [P_x \, P_y]^T$ consists of an elastic-hardening component and a hysteretic component, given by:

$$\mathbf{P} = K_2\mathbf{u} + \mathbf{F}_p \tag{8}$$

where $\mathbf{u}$ is vector of the two directional displacements, the rate of plastic force $\mathbf{F}_p$ is approximated with:

$$\dot{\mathbf{F}}_p = (K_1 - K_2)\dot{\mathbf{u}} - \frac{||\mathbf{F}_p||^{\eta-2}}{Q_D}(K_1 - K_2)\left(\mathbf{F}_p^{\mathbf{T}}\dot{\mathbf{u}}\right)\frac{1 + \text{sgn}\left(\mathbf{F}_p^{\mathbf{T}}\underline{\mathbf{u}}\right)}{2}\mathbf{F}_p \tag{9}$$

where the variable $\eta > 0$ describes the smoothness of the transition. Different isolation devices possess different Bouc–Wen behaviors in terms of the transition smoothness parameter. Specifically, η is set to be 2 for elastomeric bearings, 4 for lead rubber bearings and 8 or above for friction pendulum bearings. Defining a dimensionless plastic variable $\mathbf{Z}$ such that $\mathbf{Z} = \mathbf{F}_p/Q_D$ and the uniaxial "yield" displacement $u^Y = Q_D/(K_1 - K_2)$, Eq. (9) can be reformed as:

$$\dot{\mathbf{Z}}u^Y = A\dot{\mathbf{u}} - ||\mathbf{Z}||^{\eta-2} \times (\mathbf{Z}^{\mathbf{T}}\dot{\mathbf{u}})[\gamma + \beta\text{sgn}(\mathbf{Z}^{\mathbf{T}}\dot{\mathbf{u}})]\mathbf{Z} \tag{10}$$

where A, β, γ, and η are dimensionless quantities that control the shape of the hysteretic loop. In this study, $A = 1$ and $\beta = \gamma = 0.5$. This results in the bound of variable $\mathbf{Z}$ as $||\mathbf{Z}|| \leq 1$.

Such Bouc–Wen model has been proved versatile for modeling various seismic protection devices, such as sliding, elastomeric, or lead-rubber bearings. Figure 5 illustrates the cyclic behaviors of the three types of isolation devices under the KGM motion of the 1995 Kobe earthquake. For the friction pendulum system, especially for the triple pendulum isolators, the hardening (or stiffening) behavior at a larger strain level could be easily modeled with the provided OpenSees element by existing studies (Fenz and Constantinou 2008; Dao and Ryan 2014).

Finally, uncertainties such as heating, aging, contamination, rate-dependent effect, seasonal temperature change will all effect the ultimate performance of the isolated structure. For the heating problem, for example, Kalpakidis et al. (2010) has done a
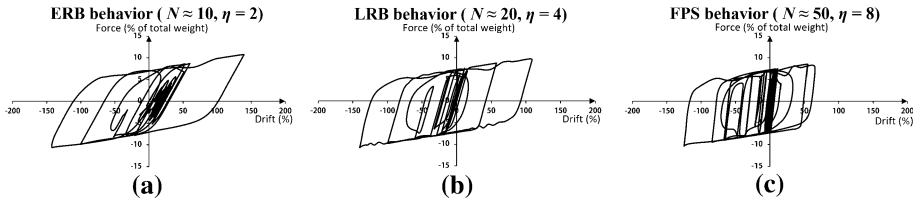
Fig. 5 Simulated dynamic behaviors for different isolation systems in major direction under KGM record of the 1995 Kobe earthquake: **a** ERB performance, **b** LRB performance, **c** FPS performance

bounded analysis for the lead rubber bearings. Their research shows that for the earthquake records with more than 3 obvious cycles, the strength degradation effect is not negligible due to the temperature increase in the lead core. In addition, such effect is not substantial and the bearings maintain their characteristic strength against the pulse-type near fault ground motions. In this study, as the selected earthquakes are the pulse-type ground motions and the far-field motions, the heating effect is not included in the study. Moreover, to evaluate the structural performance at the system level, the study has a limit that the various aforementioned uncertainties are not considered and only the basic features of the isolation system is modeled.

3.3 Modeling of the structure

A detailed 3D structural model was generated in OpenSees and nonlinear dynamic response history analyses were conducted using the selected ground motions. The 3D model simulates all the structural members with displacement-based fiber elements considering nonlinear spreading along the elements. The steel elements are assumed to have uniaxial bilinear flexural material behavior with kinematic hardening property defined by the steel01 material in OpenSees. The deteriorating properties and the collapse features are not added to the elements of the super structure as it usually remain elastic after being isolated. Ignoring the deteriorating properties might lead to smaller peak inter-story drifts and larger floor accelerations for the fixed-base situation against some big earthquake excitations. However, as the target of this study is to explore the optimum range of the base isolators of the isolated structure, deteriorating is not considered for higher computational efficiency. Five-point Gauss–Lobatto integration was assigned to the elements to increase modeling accuracy. Inelastic sections were used aggregating the axial, flexural, and torsional stiffness. Within the OpenSees model, the "corotational" geometric transfer is selected for the beams and columns considering larger deformation against major earthquake ground motions.

The predicted structural responses from the 3D model closely matched with the tested responses provided in the Blind Analysis Contest (2011). To facilitate the fragility analysis and the extensive parametric study that follows, a simplified model is derived and calibrated with the original 3D model as shown in Fig. 6a. The story stiffness K_1–K_5 still follows the bilinear relationship and provides 2.5% of the elastic stiffness after yielding. To model the triple pendulum systems, in addition to the bilinear features provided by the developed Bouc–Wen model, a nonlinear elastic hardening behavior is added after 135% shear strain of the isolator to capture the hardening effect (Fenz and Constantinou 2008). The hardening element makes the triple pendulum isolators very stiff at nearly 250% shear strain representing a locked condition. This hardening effect is removed while considering
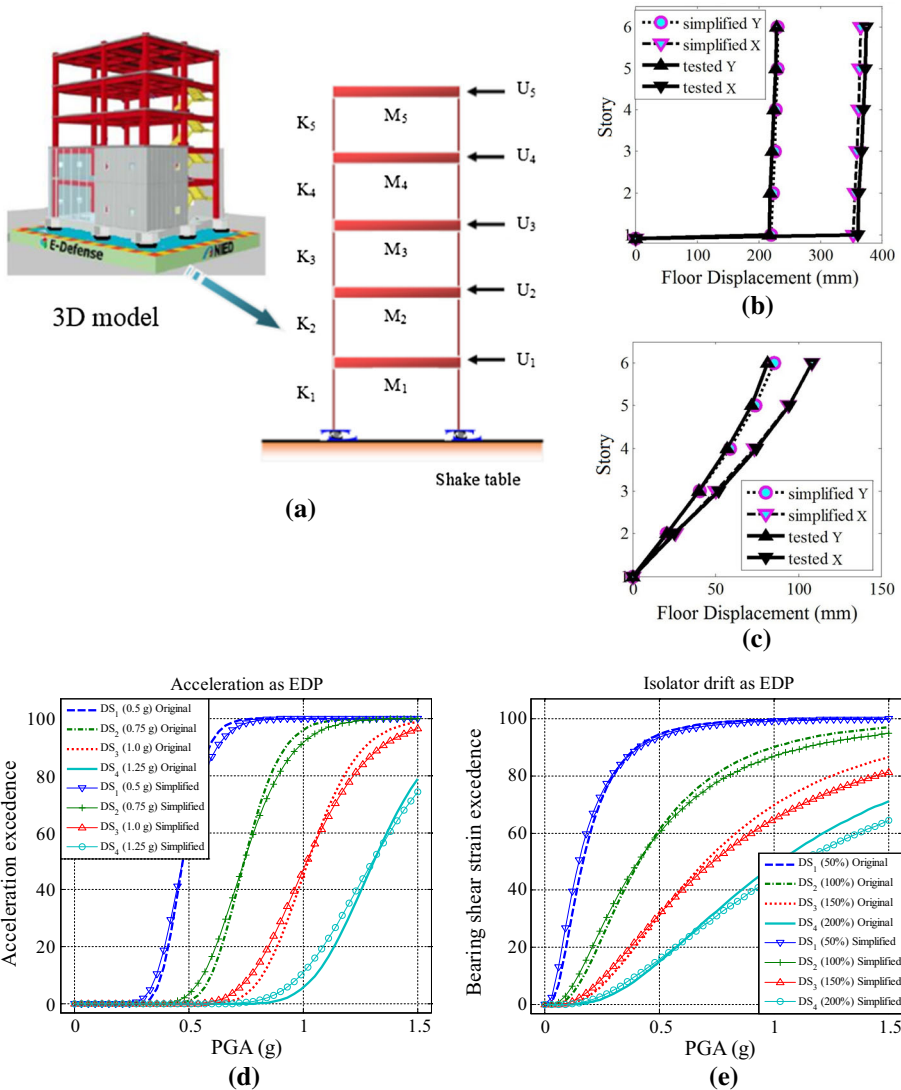
Fig. 6 Model simplification, calibration, and component level fragility curves: **a** 3D model and simplified models for the tested structure—Y direction, **b** max story displacement (isolated), **c** max story displacement (fixed-base), **d** total acceleration fragility, **e** bearing shear strain fragility

generalized isolation systems. Figure 6b, c compares the predicted floor displacements from the simplified model with the full scale tested results for both base isolated and fixed-base building subject to the Iwanuma record of the 2011 Tohoku earthquake. Subsequently, the fragility curves from the simplified and the detailed 3D model are also compared in Fig. 6d (roof level acceleration) and Fig. 6e (bearing displacement). The good match further confirms the modeling accuracy of the simplified model with the original 3D model, which is adopted for the subsequent analyses.

3.4 Fragility analyses

Fragility analyses are conducted with the developed simplified building model to investigate the optimal design of isolation devices subject to the suite of earthquake motions. The simplified OpenSees model is also a 3D model whose isolation system is modeled with the two-horizontal directions coupled Bouc–Wen behavior. Nonetheless, for the *EDP*s such as the inter-story drifts, the floor accelerations, and the isolation shear strains, the study only measures the larger value instead of the vector norm out of the two directions during each earthquake excitation. Figure 7 illustrates the relationship between the computed *EDP*s and the corresponding PGA (unit in g) of ground motions in logarithmic scale. The closer each point gets to the regressed linear line, the better *EDP* and *IM* are correlated, indicating better regression results.

Figure 8 shows the acceleration and bearing shear strain fragility curves for the originally-designed isolated building. The building inter-story drift fragility curve is not presented here due to their extremely small values, indicating negligible SC loss after using the base isolation (i.e. $P^{st} \approx 0$). To compute the *TLR* under very rare earthquakes (i.e. mean PGA = 0.82 g), the first step is to compute the bonded damage probability from the fragility curves, i.e. $P^{ns} = [0, 88.2\%, 11.8\%, 0]$ and $P^{iso} = [24.7, 20.8, 15.3, 23.9\%]$ respectively. From Table 3, the repair percentage $r^{st} = r^{ns} = r^{iso} = [2, 10, 50, 100\%]$ for the four damage states. Then, the *TLR* could be computed from Eq. (7) as:

$$TLR_{|PGA=0.82g} = \frac{\sum_{i=1}^{4} P_{(i)}^{st} r_{(i)}^{st} + \alpha \sum_{i=1}^{4} P_{(i)}^{ns} r_{(i)}^{ns} + \beta \sum_{i=1}^{4} P_{(i)}^{iso} r_{(i)}^{iso}}{1 + \alpha + \beta} \xrightarrow[P^{st} \approx 0]{\alpha = 1.0, \beta = 0.08} 8.39\%$$

$$(11)$$

4 Optimum design of the isolation system

Following the calibrated numerical model and the established PBEE framework, the study proceeds to a systematic investigation of the mechanical properties of isolation devices on the structural responses, potential damages, and essentially the *TLR* of an isolated building. Particularly, a parametric study has been conducted to explore the optimum design range for isolation system. For each design of isolation system, the fragility curves are generated
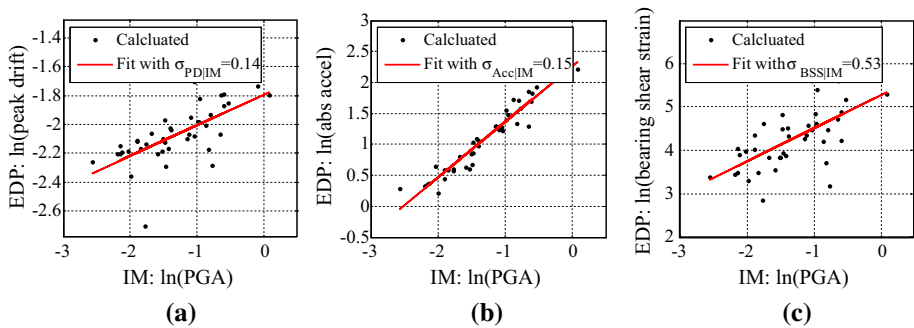

Fig. 7 Simulated *EDP*s as function of PGA (*IM*s): **a** inter-story drifts, **b** total acceleration **c** bearing shear strain
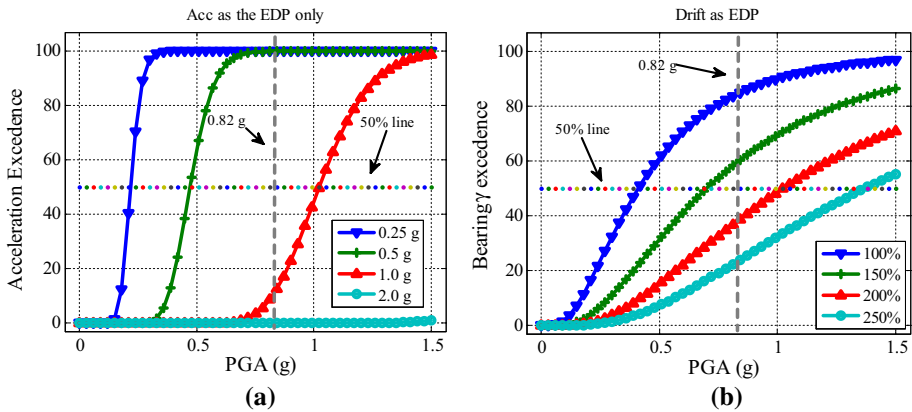
Fig. 8 Fragility curves for the code-designed base isolated structure: **a** total acceleration fragility curve, **b** bearing shear strain fragility curve

and then used to compute the *TLR* as the system level performance index for the given isolation design. An array of isolation systems with various combinations of model parameters are selected for the parametric study. The isolation devices have the stiffness ratios N of 10, 20, and 50 respectively to represent the three common isolation types. For each given stiffness ratio, the post-yielding stiffness K_{2_I} for the isolation system is varied from 0.01 to 0.08 times of the building elastic stiffness K_{1_B}, and the bearing yielding strength Q_{d_I} is varied from 0.03 to 0.45 times the building yielding strength Q_{d_B}. The seismic hazard levels are dependent on-site locations. For the location and site where the building is hypothetically designed, a basic seismic hazard analysis has been performed, where four different hazard levels are considered in the parametric study according to the approach recommended by Haselton et al. (2007). As an example, Table 5 lists the four site dependent hazard levels and their mean PGAs from the uniform hazard analysis. Referring to the corresponding value of each hazard level of *IM* from Table 5, the fragility probabilities of four damage states for each of the *EDP*s could be obtained. Finally, according to Eq. (7), the *TLR* for each hazard level is computed, recorded and compared to facilitate the performance based design of the base isolation system.

For demonstration purpose, Fig. 9 plots the *TLR* as the function of Q_{d_I}/Q_{d_B} and K_{2_I}/K_{1_B} under a suite of far-field motions that represents a 20% in 5 years hazard level. The isolation devices have a stiffness ratio of $N = 20$ while the *TLR* is computed assuming zero NSC cost (i.e. $\alpha = 0$). The deeper points on the contour is marked with darker colors, indicating better performances. The deepest point on the contour represents the smallest *TLR* at the given hazard level, which also corresponds to the lowest fragility that incurs the

Table 5 Hazard levels and their mean PGA from uniform hazard analysis

Hazard level	20% in 5 years Frequent	10% in 50 years Rare	2% in 50 years Very rare	Catastrophic Extremely rare
Equivalent mean return period	22	475	2475	Unpredictable
Mean PGA	0.20 (g)	0.55 (g)	0.82 (g)	1.20 (g)

Fig. 9 Influence of Q_{d_I} and K_{2_I} of isolation devices ($N = 20$) on *TLR* with far-field motions and $\alpha = 0.0$ at 20%-in-5-years hazard level
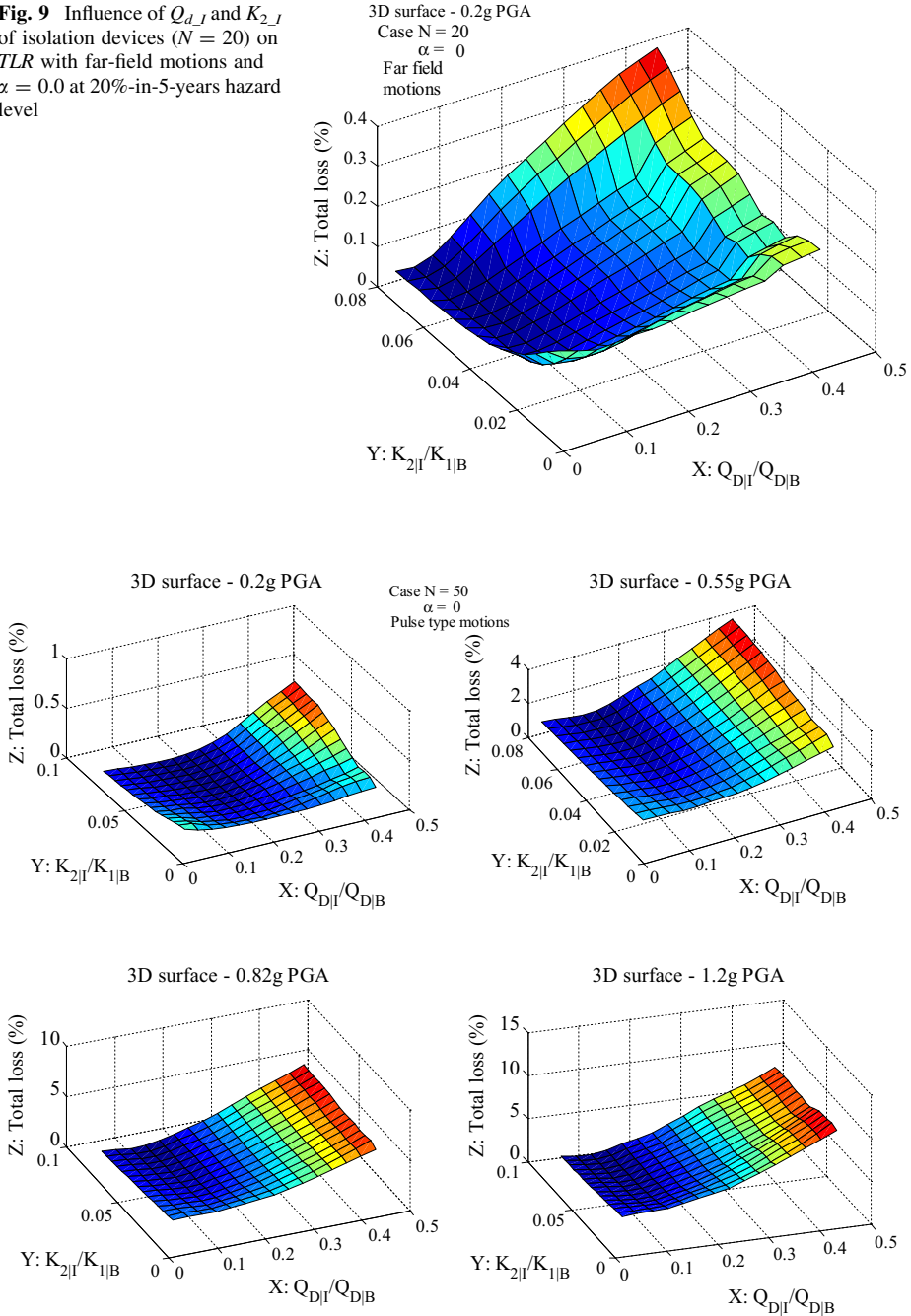

Fig. 10 Influence of Q_{d_I} and K_{2_I} of isolation devices (N = 50) on *TLR* with pulse-type motions and $\alpha = 0.0$ at different hazard levels

best structural performances. The model parameters corresponding to the bottom (optimized) point therefore represent the optimal design of the isolation system. Similarly, Fig. 10 shows *TLR* surfaces for pulse-type motions with non-structural parameter $\alpha = 0$ and bearing stiffness ratio of $N = 50$ (close to the tested FPS bearings). In addition, four figures are presented to incorporate different hazard levels at PGA of 0.2, 0.55, 0.82, and 1.2 g. In this case, considering all the hazard levels, the optimal isolation design parameters are approximately $Q_{d\_I} = 0.12 \, Q_{d\_B}$ and $K_{2\_I} = 0.08 \, K_{1\_B}$.

Following similar steps, full sets of *TLR* contours are derived considering different non-structural parameter α, earthquake hazard levels, isolation types (i.e. stiffness ratio N), and suite of near fault and far field ground motions. The approximate optimal isolation parameters as identified by the bottom points on these plots are summarized in Tables 6 and 7 for pulse-type motions and far-field motions respectively. The data presented in the tables indicate that the optimum isolation parameters are not sensitive to the stiffness ratio N (i.e. the isolation type). The optimal characteristic strength Q_{d_I} of isolation devices is averaged around 10% of building's characteristic strength Q_{d_B}. Under pulse-type motions and without considering NSCs (i.e. $\alpha = 0$), a larger Q_{d_I} up to 0.21 of Q_{d_B} might be required. However, since the non-structural damage is usually inevitable, the optimal range of Q_{d_I} is typically around 3–12% of Q_{d_B}, which corresponds to the isolation strength to building weight ratio between 2.37 and 9.48%. It is noted that low hazard level (e.g. PGA of 0.20 g case) may result in different optimum isolation designs compared with the higher hazard levels as the damages of the isolation devices become relatively more significant affecting the *TLR* when the hazard levels are small. Another interesting observation is that when considering NSCs, the optimal selection of the post-yielding bearing stiffness K_{2_I} is recommended to be small. For example, K_{2_I} is suggested to be 1–3% of structural elastic stiffness K_{1_B}, which corresponds to an effective isolation period greater than 3.15 s. Such observation also confirms the effectiveness of the isolators as their replacement costs are relatively low such that the bearing designs with more ductility (i.e. smaller K_{2_I}) help better protect the superstructure and the NSCs.

Despite the small variability of optimal isolation parameters for different cases, it can be concluded that the bearings with $Q_{d\_I} = (0.03 \sim 0.12) \, Q_{d\_B}$ and $K_{2\_I} = (0.01 \sim 0.03) \, K_{1\_B}$ are good choices for retrofitting the prototype building. The designed isolation system, which has $Q_{d\_I}/Q_{d\_B} = 9.2\%$ and $K_{2\_I}/K_{1\_B} = 0.03$, provides a reasonable design near the optimized range identified in this study. Another observation is that K_{1_I}/K_{1_B} increases proportionally with stiffness ratio N. Since the elastic stiffness K_{1_I} is N times the post-yielding stiffness K_{2_I}, the results once more imply that K_{1_I} is insignificant whereas K_{2_I} plays a much more crucial role for optimal design of isolation devices. This matches the isolator design theory where the post yielding stiffness K_{2_I} and the characteristic strength Q_{d_I} dominates the bearing behavior for severe ground motions.

The minimum *TLRs* with optimal isolation parameters are summarized in Tables 8 and 9 for pulse-type motions and for far-field motions, respectively. The *TLR* increases as the earthquake intensity increases. By comparing *TLRs* for buildings with different non-structural values (i.e. $\alpha = 0, 0.5, 1.0$), it is noted that the majority seismic loss of the isolated building comes mainly from the repair cost of NSCs. This is because the isolation design significantly reduces the inter-story drifts (i.e. eliminating the structural damages) whereas the fixed base structure incur significant damages in both SCs and NSCs (see Table 10). Notice that the *TLR* of the fixed base structure could be less accurate than the isolated structures as the strength deterioration was not considered in the numerical structural model. The results also show that near-fault motions result in higher *TLR* than the far-field motions. Moreover, it has been proved again that when K_{2_I} fixed at a specific

Table 6 Optimal range for design variables when structure subject to pulse-type motions

	0.20 (g)	0.55 (g)	0.81 (g)	1.20 (g)	Range
Stiffness ratio $N = K_{1\_I}/K_{2\_I} = 10$					
$\alpha = 0.0$					
Q_{D_I}/Q_{D_B}	0.21	0.15	0.12	0.09	0.09–0.21
K_{2_I}/K_{1_B}	0.08	0.08	0.08	0.08	0.08–0.08
K_{1_I}/K_{1_B}	0.8	0.8	0.8	0.8	0.8–0.8
$\alpha = 0.5$					
Q_{D_I}/Q_{D_B}	0.03	0.03	0.03	0.03	0.03–0.03
K_{2_I}/K_{1_B}	0.01	0.01	0.01	0.01	0.01–0.01
K_{1_I}/K_{1_B}	0.1	0.1	0.1	0.1	0.1–0.1
$\alpha = 1.0$					
Q_{D_I}/Q_{D_B}	0.06	0.03	0.03	0.03	0.03–0.06
K_{2_I}/K_{1_B}	0.01	0.01	0.01	0.015	0.01–0.015
K_{1_I}/K_{1_B}	0.1	0.1	0.1	0.15	0.1–0.15
Stiffness ratio $N = K_{1\_I}/K_{2\_I} = 20$					
$\alpha = 0.0$					
Q_{D_I}/Q_{D_B}	0.18	0.15	0.12	0.09	0.09–0.18
K_{2_I}/K_{1_B}	0.08	0.08	0.08	0.08	0.08–0.08
K_{1_I}/K_{1_B}	1.6	1.6	1.6	1.6	1.6–1.6
$\alpha = 0.5$					
Q_{D_I}/Q_{D_B}	0.12	0.03	0.03	0.03	0.03–0.12
K_{2_I}/K_{1_B}	0.01	0.01	0.01	0.01	0.01–0.01
K_{1_I}/K_{1_B}	0.2	0.2	0.2	0.2	0.2–0.2
$\alpha = 1.0$					
Q_{D_I}/Q_{D_B}	0.06	0.03	0.03	0.03	0.03–0.06
K_{2_I}/K_{1_B}	0.01	0.01	0.01	0.01	0.01–0.01
K_{1_I}/K_{1_B}	0.2	0.2	0.2	0.2	0.2–0.2
Stiffness ratio $N = K_{1\_I}/K_{2\_I} = 50$					
$\alpha = 0.0$					
Q_{D_I}/Q_{D_B}	0.18	0.12	0.12	0.09	0.09–0.18
K_{2_I}/K_{1_B}	0.08	0.08	0.08	0.08	0.08–0.08
K_{1_I}/K_{1_B}	4	4	4	4	4–4
$\alpha = 0.5$					
Q_{D_I}/Q_{D_B}	0.03	0.03	0.03	0.03	0.03–0.03
K_{2_I}/K_{1_B}	0.03	0.01	0.01	0.01	0.01–0.03
K_{1_I}/K_{1_B}	1.5	0.5	0.5	0.5	0.5–1.5
$\alpha = 1.0$					
Q_{D_I}/Q_{D_B}	0.03	0.03	0.03	0.03	0.03–0.03
K_{2_I}/K_{1_B}	0.01	0.01	0.01	0.01	0.01–0.01
K_{1_I}/K_{1_B}	0.5	0.5	0.5	0.5	0.5–0.5

range, the stiffness ratio N has negligible effect to the building response reflected by almost identical *TLR*s at given earthquake intensity.

Table 10 compares the *TLR*s for the fixed-base and the base-isolated building with different isolation designs. Assuming that the NSC costs the same as the SC (i.e. $\alpha = 1.0$),

Table 7 Optimal range for design variables when structure experiences far-field motions

	0.20 (g)	0.55 (g)	0.81 (g)	1.20 (g)	Range
Stiffness ratio N = K_{1_I}/K_{2_I} = 10					
$\alpha = 0.0$					
Q_{D_I}/Q_{D_B}	0.06	0.03	0.03	0.03	0.03–0.06
K_{2_I}/K_{1_B}	0.08	0.08	0.08	0.08	0.08–0.08
K_{1_I}/K_{1_B}	0.8	0.8	0.8	0.8	0.8–0.8
$\alpha = 0.5$					
Q_{D_I}/Q_{D_B}	0.03	0.03	0.03	0.03	0.03–0.03
K_{2_I}/K_{1_B}	*0.01*	*0.08*	*0.02*	*0.02*	0.01–0.08
K_{1_I}/K_{1_B}	0.1	0.8	0.2	0.2	0.1–0.8
$\alpha = 1.0$					
Q_{D_I}/Q_{D_B}	0.03	0.03	0.03	0.03	0.03–0.03
K_{2_I}/K_{1_B}	0.01	0.01	0.02	0.02	0.01–0.02
K_{1_I}/K_{1_B}	0.1	0.1	0.2	0.2	0.1–0.2
Stiffness ratio N = K_{1_I}/K_{2_I} = 20					
$\alpha = 0.0$					
Q_{D_I}/Q_{D_B}	0.06	0.03	0.03	0.03	0.03–0.06
K_{2_I}/K_{1_B}	0.065	0.08	0.08	0.08	0.065–0.08
K_{1_I}/K_{1_B}	1.3	1.6	1.6	1.6	1.3–1.6
$\alpha = 0.5$					
Q_{D_I}/Q_{D_B}	0.03	0.03	0.03	0.03	0.03–0.03
K_{2_I}/K_{1_B}	*0.02*	*0.045*	*0.01*	*0.08*	0.01–0.08
K_{1_I}/K_{1_B}	0.4	0.9	0.2	1.6	0.2–1.6
$\alpha = 1.0$					
Q_{D_I}/Q_{D_B}	0.03	0.03	0.03	0.03	0.03–0.03
K_{2_I}/K_{1_B}	*0.01*	*0.01*	*0.01*	*0.08*	0.01–0.08
K_{1_I}/K_{1_B}	0.2	0.2	0.2	1.6	0.2–1.6
Stiffness ratio N = K_{1_I}/K_{2_I} = 50					
$\alpha = i0.0$					
Q_{D_I}/Q_{D_B}	0.03	0.03	0.03	0.03	0.03–0.03
K_{2_I}/K_{1_B}	0.08	0.08	0.08	0.08	0.08–0.08
K_{1_I}/K_{1_B}	4	4	4	4	4–4
$\alpha = 0.5$					
Q_{D_I}/Q_{D_B}	0.03	0.03	0.03	0.03	0.03–0.03
K_{2_I}/K_{1_B}	0.01	0.02	0.03	0.03	0.01–0.03
K_{1_I}/K_{1_B}	0.5	1	1.5	1.5	0.5–1.5
$\alpha = 1.0$					
Q_{D_I}/Q_{D_B}	0.03	0.03	0.03	0.03	0.03–0.03
K_{2_I}/K_{1_B}	0.01	0.01	0.03	0.03	0.01–0.03
K_{1_I}/K_{1_B}	0.5	0.5	1.5	1.5	0.5–1.5

The tilted data implies that a wide range close to the values is also close to optimal

the originally-designed isolation devices (ASCE 7-10 2010; Dao et al. 2013; Dao and Ryan 2014) in the test structure reduced the *TLR* from 4.9% to almost zero under small yet frequent earthquake input motions (e.g. 20% in 5 years, PGA = 0.2 g), while the *TLR* was reduced from 53.8 to 8.39% under very rare earthquake input motions (e.g. 2% in 50 years,

Table 8 Minimum *TLR*s under pulse-type motions (in %)

			0.20 (g)	0.55 (g)	0.82 (g)	1.20 (g)
Stiffness ratio N = K_{1_I}/K_{2_I} = 10						
$\alpha = 0.0$	Minimum loss	0.05	0.87	1.86	3.17
$\alpha = 0.5$	Minimum loss	0.16	1.72	4.62	21.22
$\alpha = 1.0$	Minimum loss	0.22	1.99	6.33	25.46
Stiffness ratio N = K_{1_I}/K_{2_I} = 20						
$\alpha = 0.0$	Minimum loss	0.05	0.65	1.50	2.66
$\alpha = 0.5$	Minimum loss	0.16	1.69	4.50	21.29
$\alpha = 1.0$	Minimum loss	0.22	1.92	6.42	25.22
Stiffness ratio N = K_{1_I}/K_{2_I} = 50						
$\alpha = 0.0$	Minimum loss	0.01	0.46	1.22	2.36
$\alpha = 0.5$	Minimum loss	0.15	1.69	4.54	22.38
$\alpha = 1.0$	Minimum loss	0.23	1.94	6.38	25.90

Table 9 Minimum *TLR*s under far-field motions (in %)

			0.20 (g)	0.55 (g)	0.82 (g)	1.20 (g)
Stiffness ratio N = K_{1_I}/K_{2_I} = 10						
$\alpha = 0.0$	Minimum loss	0.02	0.39	0.91	1.83
$\alpha = 0.5$	Minimum loss	0.13	1.04	1.96	14.12
$\alpha = 1.0$	Minimum loss	0.14	1.22	2.60	17.83
Stiffness ratio N = K_{1_I}/K_{2_I} = 20						
$\alpha = 0.0$	Minimum loss	0.06	0.37	0.84	1.66
$\alpha = 0.5$	Minimum loss	0.14	1.05	1.88	16.79
$\alpha = 1.0$	Minimum loss	0.15	1.23	2.58	18.00
Stiffness ratio N = K_{1_I}/K_{2_I} = 50						
$\alpha = 0.0$	Minimum loss	0.04	0.30	0.77	1.61
$\alpha = 0.5$	Minimum loss	0.13	1.05	1.95	16.41
$\alpha = 1.0$	Minimum loss	0.15	1.24	2.54	18.14

Table 10 *TLR*s for different designs with 100 motions and $\alpha = 1.0$ (in %)

Case	0.2 (g)	0.55 (g)	0.82 (g)	1.20 (g)
Fixed	4.90	34.10	53.84	71.13
Designed	0.43	5.24	8.39	29.46
Optimal when N = 10	0.18	1.69	4.72	22.80
Optimal when N = 20	0.19	1.61	4.49	22.85
Optimal when N = 50	0.18	1.62	4.57	22.57

PGA = 0.82 g). It is further noticed that the optimal isolation design results in an even better reduction of *TLR*. A remarkable 50% performance improvement can be achieved from such performance-based design over the code-designed isolation system for the test building.

5 Conclusions

This study applies the performance-based methodology to assess the seismic performance of the base isolated mid-rise SMF and to optimally design the isolation devices to reduce overall seismic loss. Adopting a fully tested SMF structure on E-Defense shake table, the detailed and simplified numerical models were developed and calibrated with experimental data. Under the PBEE framework, the total loss ratio (TLR) is implemented as the system level performance index considering damages for structural, non-structural and isolation components. Fragility curves are generated and utilized to derive the TLR. A comprehensive parametric study is subsequently carried out to consider various earthquake hazard levels, isolation designs, and both structural and non-structural damages, etc. Finally, the optimal isolation parameters are identified that correspond to the lowest TLR.

The study demonstrates that the TLR is an effective performance index quantifying the system level seismic performance of isolated buildings. It combines the repair costs and the component level probabilistic performance of structural components (SC) and non-structural components (NSC) as well as isolation devices. Furthermore, the optimal isolation parameters corresponding to the lowest TLR are functions of structural properties and damage states. The structure will experience minimum overall damage when the characteristic strength Q_{d_I} of isolation devices is about 3–12% of structural strength Q_{d_B} (the strength to building weight ratio between 2.37 and 9.48%) and the post-yielding stiffness K_{2_I} is about 1–3% K_{1_B} (the effective period of isolation system longer than 3.15 s). The overall damage potential is not sensitive to the elastic stiffness of isolation devices. The results comparing TLRs for fixed-base and base isolated buildings also show the significant performance improvement due to isolation especially when NSCs (i.e. building contents) are of similar values to SCs.

In summary, the study offers a systematic way to select optimal isolation device parameters based on structural properties and performance objectives while incorporating the uncertainties in ground motions and variability of structural properties under the fragility function framework.

References

ASCE (2010) ASCE 7-10 minimum design loads for buildings and other structures. American Society of Civil Engineers, Reston

Aslani H, Miranda E (2005) Probabilistic earthquake loss estimation and loss disaggregation in buildings. Technical Report No. 157, The John A. Blume Earthquake Engineering Center, Stanford University, Stanford

ATC (1996) ATC-40 seismic evaluation and retrofit of concrete buildings. SSC 96-01, Seismic Safety Commission, Project 40, Applied Technology Council, Redwood City

ATC (2012) ATC-58 seismic performance assessment of buildings. FEMA P-58, Applied Technology Council, Redwood City

Bai JW, Hueste MB, Gardoni P (2009) Probabilistic assessment of structural damage due to earthquakes for buildings in mid-America. J Struct Eng ASCE 135(10):1155–1163

Blind Analysis Contest (2011) Numerical prediction of shaking table test of 5-story steel frame with and without base isolation. http://www.cuee.titech.ac.jp/contest/

Bouc R (1971) Modele mathematique d'hysteresis. Acustica 24:16–25

Casciati F (1989) Stochastic dynamics of hysteretic media. Struct Safety 6(2–4):259–269

Dao ND, Ryan KL (2014) Computational simulation of a full-scale, fixed-base, and isolated-base steel moment frame building tested at E-Defense. J Struct Eng ASCE Spec Issue Comput Simul Struct Eng 140:A4014005

Dao ND, Ryan KL, Sato E, Sasaki T (2013) Predicting the displacement of triple pendulum bearings in a full scale shaking experiment using a three-dimensional element. Earthquake Eng Struct Dyn 42(11):1677–1695

Dhakal RP, Mander JB (2006) Financial risk assessment methodology for natural hazards. Bull N Z Soc Earthq Eng 39(2):91–105

Fajfar P, Gašperšič P (1996) The N2 method for the seismic damage analysis of RC buildings. Earthq Eng Struct Dyn 25:31–46

FEMA (1997a) FEMA 273 NEHRP guidelines for seismic rehabilitation of buildings. Federal Emergency Management Agency, Washington

FEMA (1997b) FEMA 274 NEHRP commentary on the guidelines for seismic rehabilitation of buildings. Federal Emergency Management Agency, Washington

FEMA (2003) Multi-hazard loss estimation methodology—earthquake model. HAZUS-MH MR4 Technical Manual, Federal Emergency Management Agency, Washington

Fenz DM, Constantinou MC (2008) Modeling triple friction pendulum bearings for response-history analysis. Earthq Spectra 24(4):1011–1028

Graf WP, Lee Y (2009) Code-oriented damage assessment for buildings. Earthq Spectra 25(1):17–37

Hall JF, Heaton TH, Halling MW, Wald DJ (1995) Near-source ground motion and its effects on flexible buildings. Earthq Spectra 11:569–605

Haselton CB, Goulet CA, Mitrani-Reiser J, Beck JL, Deierlein GG, Porter KA, Stewart JP, Taciroglu E (2007) An assessment to benchmark the seismic performance of a code-conforming reinforced concrete moment-frame building. PEER Report 07/12, Pacific Earthquake Engineering Research Center, University of California, Berkeley

Ji X, Hikino T, Kasai K, Nakashima M (2013) Damping identification of a full-scale passively controlled five-story steel building structure. Earthq Eng Struct Dyn 42(2):277–295

Kalpakidis IV, Constantinou M, Whittaker A (2010) Modeling strength degradation in lead-rubber bearing under earthquake shaking. Earthquake Eng Struct Dyn 39(13):1533–1549

Kasai K, Hikino T, Ito H, Ooki Y, Motoyui S, Kato F, Baba Y (2011) Overall test outline and response of building without dampers. 3D shake table tests on full scale 5-story steel building with dampers, part 1. J Struct Constr Eng AIJ 76(663):997–1006 **(in Japanese)**

Kelly JM (1986) Aseismic base isolation: review and bibliography. Soil Dyn Earthq Eng 5(3):202–216

Kircher CA (2003) It makes dollars and sense to improve nonstructural system performance. In: ATC-29-2 proceedings of seminar on seismic design, performance, and retrofit of nonstructural components in critical facilities, Los Angeles, CA

Kumar M, Whittaker A, Constantinou M (2014) An advanced numerical model of elastomeric seismic isolation bearings. Earthq Eng Struct Dyn 43(13):1955–1974

Lafontaine M, Moroni O, Sarrazin M, Roschke P (2009) Optimal control of accelerations in a base-isolated building using magneto-rheological dampers and genetic algorithms. J Earthq Eng 13:1153–1171

Lee HJ, Yang GQ, Jung HJ, Spenser BF, Lee IW (2006) Semi-active neurocontrol of a base-isolated benchmark structure. Struct Control Health 13:682–692

Mackie KR, Stojadinović B (2005) Fragility basis for California highway overpass bridge seismic decision making. PEER Report 05/02, Pacific Earthquake Engineering Research Center, University of California, Berkeley

Mackie KR, Stojadinović B (2007) Performance-based seismic bridge design for damage and loss limits states. Earthq Eng Struct Dyn 36:1953–1971

Makris N, Vassiliou MF (2011) The existence of "complete similarities" in the response of seismic isolated structures subjected to pulse-like ground motions and their implications in analysis. Earthq Eng Struct Dyn 40:1103–1121

Makris N, Zhang J (2002) Structural characterization and seismic response analysis of a highway overcrossing equipped with elastomeric bearings and fluid dampers: a case study. PEER Report 02/17, Pacific Earthquake Engineering Research Center, University of California, Berkeley

Moon BY, Kang GJ, Kang BS, Kelly JM (2002) Design and manufacturing of fiber reinforced elastomeric isolator for seismic isolation. J Mater Process Technol 130–131:145–150

Naeim F, Kelly JM (1999) Design of seismic isolated structures: from theory to practice. Wiley, New York

Nielson BG, DesRoches R (2007) Seismic fragility methodology for highway bridges using a component level approach. Earthq Eng Struct Dyn 36(6):823–839

OpenSees (2017) Open system for earthquake engineering simulation. Pacific Earthquake Engineering Research (PEER) Center, University of California: Berkeley. http://opensees.berkeley.edu/

Padgett JE, Nielson BG, DesRoches R (2008) Selection of optimal intensity measures in probabilistic seismic demand models of highway bridge portfolios. Earthq Eng Struct Dyn 37(5):711–725

Plotner SC, Babbitt C, Charest AC, Elsmore C, Gomes J (2016) Building construction costs with RSMeans Data 2017. R.S. Means data from GORDIAN

Porter KA (2003) An overview of PEER's performance-based earthquake engineering methodology. In: Proceedings of ninth international conference on applications of statistics and probability in civil engineering, San Francisco, CA

Ryan K, Chopra A (2004) Estimation of seismic demands on isolators based on nonlinear analysis. J Struct Eng ASCE 130(3):392–402

Sabelli R, Mahin S, Chang C (2003) Seismic demands on steel braced frame buildings with buckling restrained braces. Eng Struct 25(5):655–666

Sayani PJ, Ryan KL (2009) Comparative evaluation of base-isolated and fixed-base buildings using a comprehensive response index. J Struct Eng ASCE 135(6):698–707

SEAOC (Structural Engineers Association of California) (1995) Vision 2000: performance-based seismic engineering of buildings, vols. I, II. Structural Engineers association of California, Sacramento

Shu Z, Li S, Sun X, He M (2017) Performance-based seismic design of a pendulum tuned mass damper system. J Earthq Eng. https://doi.org/10.1080/13632469.2017.1323042

Skinner RI, Robinson WH, McVerry GH (1993) An introduction to seismic isolation. Wiley, Chichester

Solberg KM, Dhakal RP, Mander JB, Bradley BA (2008) Computational and rapid expected annual loss estimation methodologies for structures. Earthq Eng Struct Dyn 37(1):81–101

Tang Y, Zhang J (2011) Response spectrum-oriented pulse identification and magnitude scaling of forward directivity pulses in near-fault ground motions. Soil Dyn Earthq Eng 31:59–76

Wen YK (1975) Approximate method for nonlinear random vibration. J Eng Mech ASCE 101(EM4):389–401

Wen YK (1976) Method for random vibration of hysteretic systems. J Eng Mech ASCE 102(EM2):249–263

Williams MS, Villemure I, Sexsmith RG (1997) Evaluation of seismic damage indices for concrete elements loaded in combined shear and flexure. ACI Struct J 94(3):315–322

Yu Y, Tsai K, Weng Y, Lin B, Lin J (2010) Analytical studies of a full-scale steel building shaken to collapse. Eng Struct 32(10):3418–3430

Yu Y, Tsai K, Li C, Weng Y, Tsai C (2013) Earthquake response analyses of a full-scale five-story steel frame equipped with two types of dampers. Earthq Eng Struct Dyn 42(9):1301–1320

Yun S, Hamburger R, Cornell C, Foutch D (2002) Seismic performance evaluation for steel moment frames. J Struct Eng ASCE Spec Issue Steel Moment Frames After Northridge 128(Part II):534–545

Zhang J, Huo Y (2009) Evaluating effectiveness and optimum design of isolation devices for highway bridges using the fragility function method. Eng Struct 31(8):1648–1660